



Phosphodiesterase 4A confers resistance to PGE₂-mediated suppression in CD25⁺/CD54⁺ NK cells

Ziqing Chen^{1,†} , Ying Yang^{1,2,3,†}, Shi Y Neo¹, Hao Shi¹ , Yi Chen¹, Arnika K Wagner⁴, Karin Larsson⁵, Le Tong¹, Per-Johan Jakobsson⁵, Evren Alici⁴, Jing Wu⁶, Yihai Cao⁶, Kai Wang³, Lisa L Liu¹, Yumeng Mao⁷, Dhifaf Sarhan⁶ & Andreas Lundqvist^{1,*} 

Abstract

Inadequate persistence of tumor-infiltrating natural killer (NK) cells is associated with poor prognosis in cancer patients. The solid tumor microenvironment is characterized by the presence of immunosuppressive factors, including prostaglandin E₂ (PGE₂), that limit NK cell persistence. Here, we investigate if the modulation of the cytokine environment in lung cancer with IL-2 or IL-15 renders NK cells resistant to suppression by PGE₂. Analyzing Cancer Genome Atlas (TCGA) data, we found that high NK cell gene signatures correlate with significantly improved overall survival in patients with high levels of the prostaglandin E synthase (PTGES). *In vitro*, IL-15, in contrast to IL-2, enriches for CD25⁺/CD54⁺ NK cells with superior mTOR activity and increased expression of the cAMP hydrolyzing enzyme phosphodiesterase 4A (PDE4A). Consequently, this distinct population of NK cells maintains their function in the presence of PGE₂ and shows an increased ability to infiltrate lung adenocarcinoma tumors *in vitro* and *in vivo*. Thus, strategies to enrich CD25⁺/CD54⁺ NK cells for adoptive cell therapy should be considered.

Keywords cancer; cell therapy; natural killer cells; phosphodiesterase; prostaglandin-E2

Subject Categories Cancer; Immunology; Signal Transduction

DOI 10.15252/embr.202051329 | Received 15 July 2020 | Revised 14 December 2020 | Accepted 21 December 2020 | Published online 22 January 2021

EMBO Reports (2021) 22: e51329

Introduction

Due to their important role in immune surveillance and eradication of tumor cells, natural killer (NK) cells are increasingly used in

cancer immunotherapy. Early studies demonstrate that allogeneic NK cells contribute to graft-versus-leukemia effects in the setting of hematopoietic stem cell transplantation (Passweg *et al*, 2004; Ruggeri *et al*, 2008). More recent studies provide evidence of therapeutic benefit with low toxicity profiles upon infusion of donor alloreactive haploidentical NK cells in patients with acute myeloid leukemia (AML) and myelodysplastic syndrome (MDS) (Shaffer *et al*, 2016; Dolstra *et al*, 2017; Bjorklund *et al*, 2018). However, infusion of NK cells in patients with solid tumors has yet to result in beneficial clinical responses. Several studies have highlighted that inadequate persistence and dysfunctionality of the infused NK cells represents rate-limiting factors for successful clinical outcome (Bachanova *et al*, 2014; Liu *et al*, 2018).

The microenvironment of solid tumors is a complex network of stromal cells consisting of several different cell types and immunosuppressive factors. In addition, specialized subsets of immunosuppressive myeloid and lymphoid cells including tumor-associated macrophages, myeloid-derived suppressor cells (MDSC), and regulatory T cells are often found in abundance within the stroma of solid tumors (Woo *et al*, 2001; Gabrilovich & Nagaraj, 2009; Solinas *et al*, 2010). Such cells and tumor cells themselves produce a variety of factors that inhibit NK cell activity (Barrow & Colonna, 2017). The arachidonic acid pathway is important in regulating inflammatory responses. Arachidonic acid is catalyzed by the cyclooxygenases (COX-1/2) into the reactive intermediate prostaglandin (PG) H₂ which is further processed into different prostaglandins, including PGE₂, by several terminal synthases. Early studies show that melanoma-derived fibroblasts produce PGE₂ to downregulate NK cell activating receptors and thereby inhibit the function of NK cells (Balsamo *et al*, 2009). More recent studies show that also other cell populations including mesenchymal stromal cells are able to inhibit NK cell function through the secretion of PGE₂ (Reinders &

1 Department of Oncology-Pathology, Karolinska Institutet, Stockholm, Sweden

2 Department of Respiratory Medicine, The Fourth Affiliated Hospital, Zhejiang University School of Medicine, Yiwu, China

3 School of Medicine, Zhejiang University, Hangzhou, China

4 Department of Medicine Huddinge, Karolinska Institutet, Stockholm, Sweden

5 Rheumatology Unit, Department of Medicine, Solna, Karolinska Institutet, Karolinska University Hospital, Stockholm, Sweden

6 Department of Microbiology, Tumor and Cell Biology, Karolinska Institutet, Stockholm, Sweden

7 Science for Life Laboratory, Department of Immunology, Genetics and Pathology, Uppsala University, Uppsala, Sweden

*Corresponding author: Tel: +46 (0) 8 517 768 59, Email: andreas.lundqvist@ki.se

†These authors contributed equally to this work

Hoogduijn, 2014; Hu *et al*, 2019). We and others have shown that tumor cells produce PGE₂ to suppress NK cell activity via the Prostaglandin E₂ receptor 2 (EP2) and EP4 receptors (Holt *et al*, 2011; Wennerberg *et al*, 2014; Li *et al*, 2016). Thus, strategies to render NK cells less susceptible to PGE₂ to increase the persistence and activity of NK cells are needed to improve clinical responses of NK cell adoptive cell therapy in patients with solid tumors.

Interleukin-2 (IL-2) and IL-15 are type I cytokines that are commonly used to activate and expand NK cells for cellular therapy. Both cytokines activate NK cells via shared beta and gamma receptors but use distinct alpha receptors to transmit signaling (Castro *et al*, 2011; Qiao & Fu, 2020). Although IL-2/IL-15 receptor complexes activate similar JAK/STAT signal transduction cascades, they display distinct activities *in vivo* where IL-2 preferentially expands regulatory T cells and CD4⁺ helper T cells and IL-15 supports the development of central memory T cells and NK cells (Zhang *et al*, 1998; Kennedy *et al*, 2000; Castro *et al*, 2011; Liao *et al*, 2011; Conlon *et al*, 2015). While activation with IL-15 or IL-2 results in similar steady-state mRNA profiles in murine CD8⁺ T cells (Ring *et al*, 2012), we recently showed that IL-15 activates mTOR and primes stress-activated gene expression programs in human NK cells (Mao *et al*, 2016). Consequently, infusion of IL-15 primed NK cells show a longer *in vivo* persistence compared with IL-2 primed NK cells.

In this study, the ability of IL-2 and IL-15 to modulate the susceptibility of NK cell to PGE₂-mediated suppression was investigated. Collectively, we found that IL-15 activates NK cells to become less susceptible to PGE₂-mediated suppression compared with IL-2. Mechanistically, our data demonstrate that IL-15 enriches for CD25⁺/CD54⁺ NK cells and this population show an mTOR-dependent upregulation of the cAMP hydrolyzing enzyme phosphodiesterase 4A (PDE4A). This population of NK cells shows increased ability to form cell clusters and kill tumor targets in the presence of PGE₂ and to infiltrate lung adenocarcinoma tumor spheroids and reduce tumor burden in zebrafish larva xenograft model. We furthermore show that high expression of *PTGES*, encoding for the enzyme responsible for PGE₂ biosynthesis, affects the prognostic value of NK cells in patients with lung adenocarcinoma. Collectively, our data position CD25⁺/CD54⁺ NK cells as a key subpopulation involved in the persistence within an immunosuppressive tumor microenvironment.

Results

Expression of PDE4A renders human NK cells less susceptible to PGE₂-mediated suppression

Since PGE₂ is abundant within the microenvironment of solid tumors and that IL-15 enhances NK cell persistence *in vivo*, we sought to investigate if NK cells activated by IL-15 or IL-2 differ in their sensitivity to PGE₂-mediated suppression. Purified NK cells from healthy individuals were activated with either IL-2 or IL-15 in the presence of PGE₂. While exposure to PGE₂ inhibited the proliferation and cytotoxicity of IL-2 activated NK cells, IL-15 activated NK cells maintained their proliferation and cytotoxicity in the presence of PGE₂. While both proliferation and cytotoxicity were significantly higher in IL-15 stimulated NK cell compared with IL-2 stimulated

NK cells in the presence of PGE₂, proliferation but not cytotoxicity was significantly higher in IL-15 stimulated NK cells in the absence of PGE₂. Yet, the difference between IL-2 and IL-15 stimulated NK cells in the presence of PGE₂ was greater than in the absence of PGE₂ (Fig 1A and B). PGE₂ did not affect the viability of either IL-2 or IL-15 activated NK cells (Fig 1C).

Through the binding to the EP2 and EP4 receptors, PGE₂ cause an increase in the production of intracellular cAMP leading to NK cell dysfunction (Holt *et al*, 2011). Hence, the concentration of intracellular cAMP was analyzed in IL-2 and IL-15 activated NK cells. Compared with IL-15, IL-2 activated NK cells showed significantly higher intracellular cAMP levels after short-term exposure to PGE₂ (Fig 1D). To investigate the underlying mechanisms of the reduced susceptibility of IL-15 activated NK cells to PGE₂, the expression of EP2 (*PTGER2*) and EP4 (*PTGER4*) receptors as well as the expression of cAMP hydrolyzing enzyme family of phosphodiesterases was analyzed. While the expression of *PTGER2* and *PTGER4* remained at similar levels in IL-2 and IL-15 activated NK cells, the expression of phosphodiesterases, and in particular *PDE4A*, was significantly higher following exposure to IL-15 (Fig 1E). The expression of PDE4A protein was confirmed to be significantly upregulated by IL-15 by flow cytometry (Fig 1F) and by immunofluorescence microscopy (Fig 1G). Selective inhibition of PDE4 significantly increased the levels of intracellular cAMP in IL-15 activated NK cells (Fig EV1A). Taken together, our results show that IL-15 activated NK cells are less susceptible to PGE₂-mediated suppression due to high expression of PDE4A accompanied by reduced intracellular levels of cAMP.

Inhibition of mTOR reduces PDE4A expression and sensitizes NK cells to PGE₂-mediated suppression

Since PDE4 is linked with mTOR activity and that mTOR plays an essential role in the activation of NK cells (Mao *et al*, 2016; Li *et al*, 2019), subpopulations of NK cells based on the expression of intracellular signaling molecules, including phosphorylation of the S6 kinase (pS6), were analyzed with regard to susceptibility to PGE₂-mediated suppression. The frequency of pS6-positive NK cells with elevated phosphorylation of AKT, STAT5, and STAT3 did not change in IL-15 activated NK cells upon exposure to PGE₂ (category 1, Fig 2A and B). In contrast, the frequency of this population of NK cells was significantly reduced in IL-2 activated NK cells upon exposure to PGE₂ (Fig EV1B). The frequency of pS6 single positive NK cells was reduced by 0.652 ± 0.094 in the presence of PGE₂ in IL-2 activated NK cells ($P = 0.0051$), while the frequency of pS6-positive IL-15 activated NK cells remained unchanged (Fig 2C).

To confirm the link between mTOR and PDE4 activity, the expression of pS6 and PDE4A was analyzed in NK cells in the presence or absence of the PDE4 inhibitor Roflumilast or the mTOR inhibitor Torin-1. Torin-1 completely reduced the frequency of pS6-positive NK (Fig EV1C), and the expression of PDE4A was significantly reduced in IL-15 activated NK cells in the presence of Torin-1 (Figs 2D and EV1D). To test whether the inhibition of mTOR would sensitize IL-15 activated NK cells to PGE₂-mediated suppression, NK cell cytotoxicity against K562 target cells was evaluated in the presence of Torin-1 and PGE₂. Indeed, the cytolytic capacity of IL-15 activated NK cells was significantly reduced upon exposure to PGE₂ in the presence of Torin-1 ($P = 0.0246$, Fig 2E). Although the

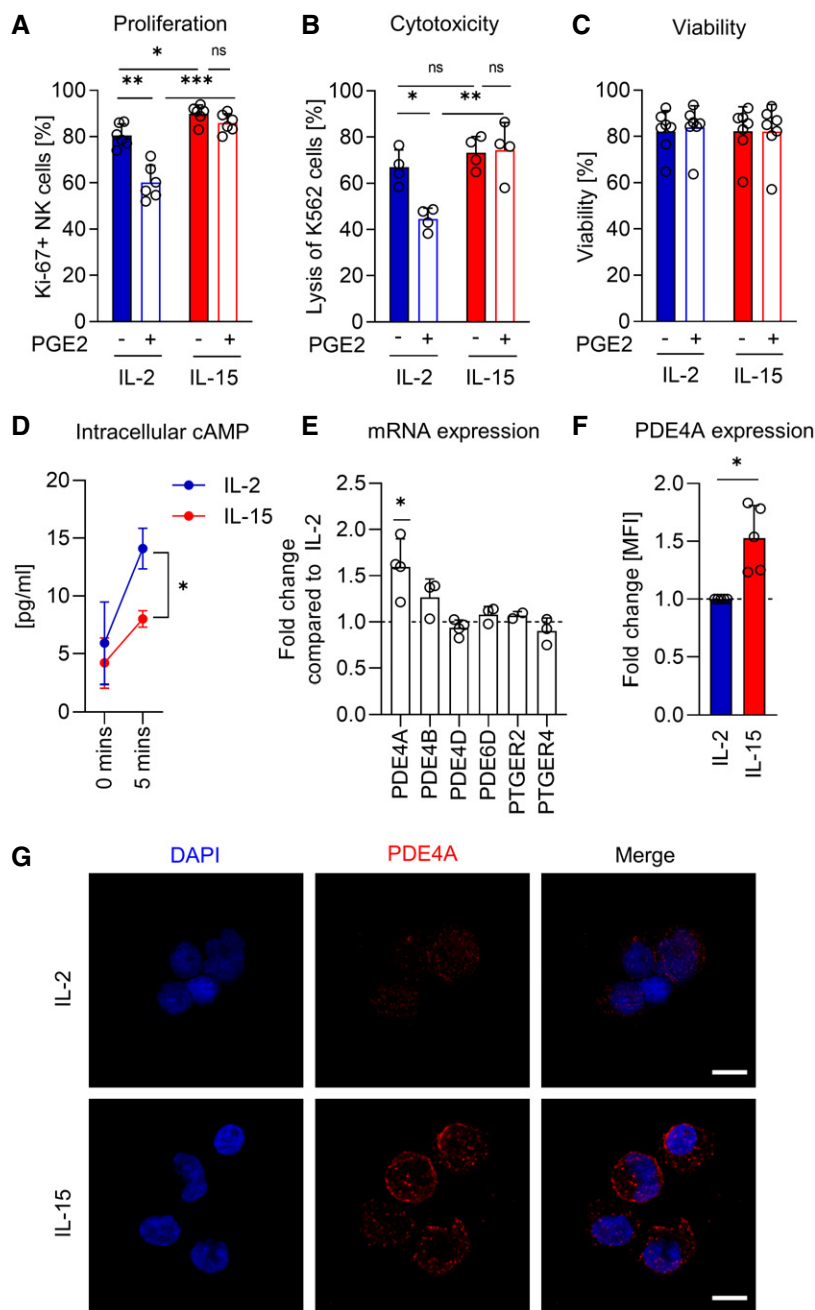


Figure 1. Expression of PDE4A renders human NK cells less susceptible to PGE₂-mediated suppression.

A–C Purified NK cells were activated with IL-2 or IL-15 in the presence or absence of PGE₂ (1 μM) and tested for (A) proliferation by flow cytometry for Ki-67 staining after 4 days of culture ($n = 6$, biological replicates), (B) ability to kill K562 cells after 2 days of culture in a 4-h chromium assay at an E:T ratio of 5:1 ($n = 4$, biological replicates). (C) Viability by flow cytometry using fixable live/dead staining after 2 days of culture ($n = 7$, biological replicates).

D Intracellular cAMP detected in 2-day IL-2 or IL-15 activated NK cells before and 5 min after the addition of PGE₂ (1 μM; $n = 3$, biological replicates).

E mRNA levels of selected PGE₂ response elements as measured by qPCR in NK cells ($n = 3–4$, biological replicates).

F Fold change comparing flow cytometry mean fluorescence intensity (MFI) values of PDE4A expression between IL-2 and IL-15 activated NK cells after 2 days activation with cytokines ($n = 5$, biological replicates).

G Representative images showing PDE4A expression in NK cells activated by IL-2 or IL-15 for 2 days. Scale bar: 10 μm.

Data information: Data were analyzed using a paired parametric *t*-test (* $P < 0.05$, ** $P < 0.01$, *** $P < 0.001$). Each circle represents an individual experiment. Error bars are depicted as standard deviation.

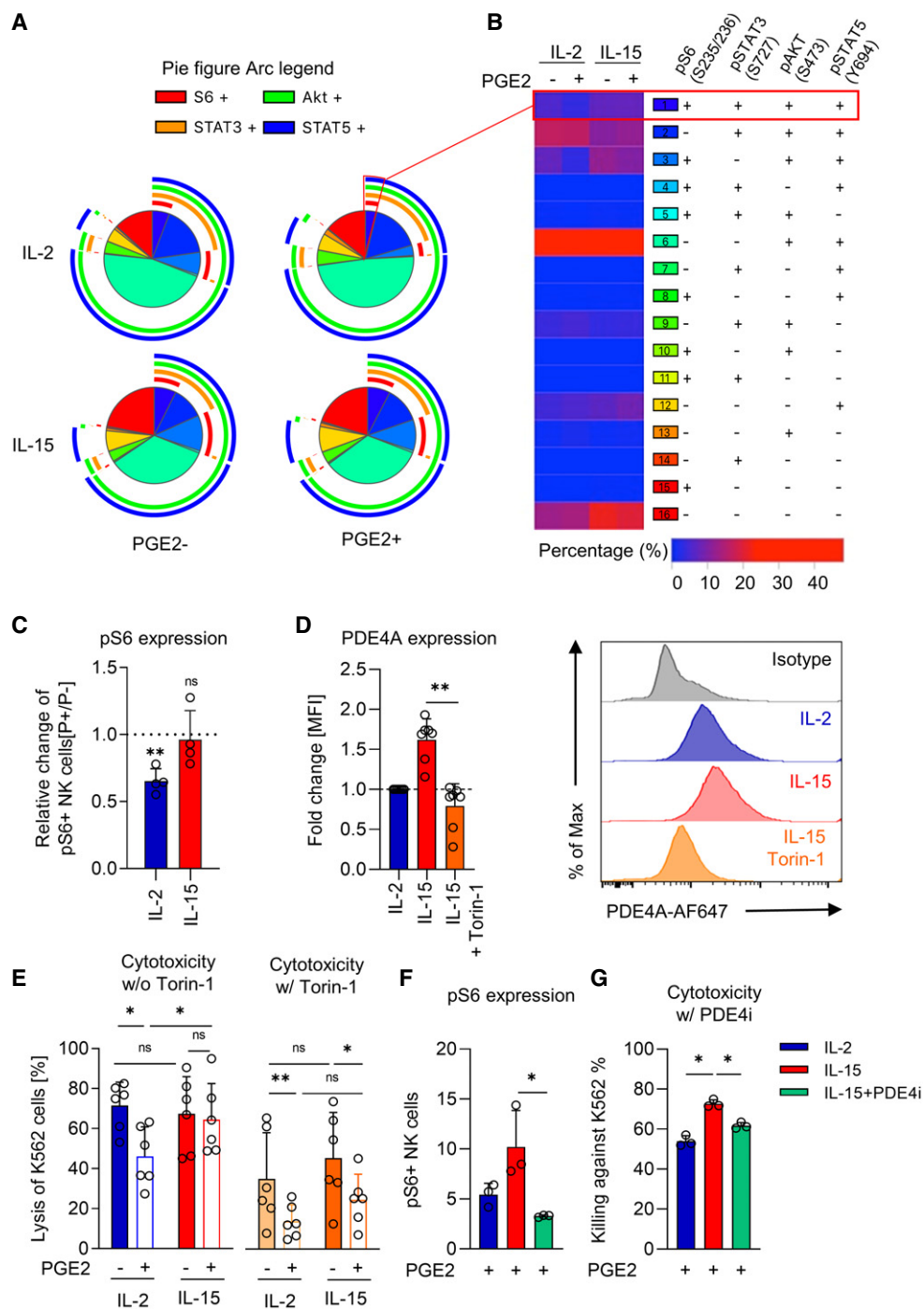


Figure 2. Inhibition of mTOR reduces PDE4A expression and sensitizes NK cells to PGE₂-mediated suppression.

A, B NK cells were activated with IL-2 or IL-15 for 2 days in the presence or absence of PGE₂ (1 μM) and analyzed for A) the levels of phosphorylated S6 (pS235/pS236), STAT3 (S727), STAT5 (Y694), Akt (S473; *n* = 4, biological replicates) and B) 16 categories of phosphorylation array showed. Red box indicates category 1 (pS6⁺, pSTAT3⁺, pSTAT5⁺, pAKT⁺).

C Relative changes in frequency of NK cells expressing pS6 in the presence and absence of PGE₂ (*n* = 4, biological replicates).

D Flow cytometry analysis of PDE4A in the presence or absence of Torin-1 (1 μM; left, *n* = 7, biological replicates) with representative histograms (right).

E NK cell-mediated cytotoxicity of K562 cells by 4-h chromium-release assay of 2-day cytokine-activated NK cells in the presence or absence of Torin-1 (1 μM) and PGE₂ (1 μM; *n* = 6, biological replicates). E:T ratio = 5:1.

F, G (F) Flow cytometry analysis of pS6 and (G) 4-h chromium-release assay of PGE₂-treated NK cells against K562 measured after 48 h treatment with Roflumilast (PDE4i, 1 μM; *n* = 3, biological replicates) E:T ratio = 5:1.

Data information: Data were analyzed using a paired parametric *t*-test (***P* < 0.05, ****P* < 0.01). Each circle represents an individual experiment. Error bars are depicted as standard deviation.

frequency of NK cells positive for pSTAT5 did not differ between IL-2 and IL-15 stimulated NK cells, IL-15 stimulation resulted in higher intensity staining for pSTAT5 (Fig EV1E). To further strengthen the association between IL-15 and PDE4A, transcription factors that bind to the PDE4A region (chr19:10,416,773–10,469,631/hg38) were analyzed by using CistromeDB toolkit. This analysis revealed several transcription factors including STAT5 to bind to the PDE4A region suggesting that IL-15 induced PDE4A expression can be regulated via JAK/STAT5 signaling (Fig EV1F).

In the presence of PGE₂, inhibition of PDE4 significantly reduced the frequency of pS6-positive IL-15 activated NK cells (Fig 2F). In addition, inhibition of PDE4 resulted in reduced killing of K562 cell by IL-15 NK cells (Fig 2G). Collectively, these results show a reciprocal cross-talk between mTOR and PDE4 activity in IL-15 activated NK cells and inhibition of either mTOR or PDE4 activity sensitizes IL-15 activated NK cells to PGE₂-mediated suppression.

IL-15 induces phenotypical changes and supports the formation of cell clustering

To comprehensively investigate differences between IL-2 and IL-15 activated NK cells, a previously published transcriptomic data set was analyzed (Mao *et al*, 2016). When enriched for immune system processes, 10 genes out of 244 differentially expressed genes (fold change > 1.5) was significantly enriched in “Positive regulation of leukocyte migration” pathway (Figs 3A and EV2A). When analyzed for the differential expression in biology process in particular for cell surface molecules (cell surface, GO:0009986) and cellular location, 27 genes were found to be differentially expressed (Fold change > 1.5). Among these, ICAM1 (CD54) and IL2-RA (CD25) were significantly higher expressed by IL-15 activated NK cells (Figs 3B and EV2B).

Flow cytometry analysis confirmed the increased expression of CD25 and CD54 and increased frequency of CD25⁺/CD54⁺ NK cells upon activation with IL-15 compared with activation with IL-2. Although not significant, the frequency of CD25⁺/CD54⁺ NK cells were reduced upon exposure to PGE₂ in both IL-2 and IL-15 activated NK cells (Fig 3C and D). Similarly, the expression of CD25 and CD54 was reduced in both IL-2 and IL-15 activated NK cells upon exposure to PGE₂. Though the expression of CD54 was not significantly reduced in IL-15 NK cells upon exposure to PGE₂. Still, the frequency of CD25⁺/CD54⁺ NK cells and the expression of CD25 and CD54 were still significantly higher in IL-15 activated NK cells compared with IL-2 activated NK cells in the presence of PGE₂ (Figs 3C and EV3A). No difference in the expression levels of CD56, CD57, CD16, NKG2A, DNAM-1, and NKP46 was observed between IL-2 and IL-15 activated NK cells. However, the expression of the activation markers CD69 and NKG2D was significantly higher in IL-15 compared with IL-2 activated NK cells (Fig EV3B).

Through binding to its ligands LFA-1, MAC-1, and fibrinogen, CD54 plays an important role in cell-to-cell interactions (Huse, 2017). Therefore, differences in the ability to form immune cell cluster were analyzed between IL-2 and IL-15 activated NK cells. Upon activation with IL-15, NK cells consistently formed distinct cell clusters even in the presence of PGE₂, while IL-2 activated NK cells displayed impaired cluster formation in the presence of with PGE₂ (Fig 3E and F). To test if the formation of cell clusters impacts on the ability of IL-15 NK cells to resist PGE₂-mediated suppression,

CD54 was blocked to prevent the formation of cell clusters (Fig EV3C). However, blockade of CD54 did not impact on the ability of IL-15 activated NK cells to kill K562 target cells in the absence or presence of PGE₂ (Fig 3G). Thus, the formation of cell clusters does not contribute to the resistance to PGE₂-mediated suppression in IL-15 activated NK cells.

Given that mTOR signaling is essential to render NK cells less susceptible to PGE₂ suppression, the impact of mTOR on the expression of CD25 and CD54 was analyzed. In the presence of Torin-1, a significant down-regulation of CD54 ($P = 0.0150$) but not CD25 ($P = 0.0964$, ns) was observed in NK cells activated by IL-15 (Fig EV3D). Blocking CD54 had no impact on the expression of pS6, pSTAT5, in IL-2 or IL-15 activated NK cells (Fig EV3E). Overall, our results demonstrate that IL-15 induces the expression of CD54 and CD25 through mTOR signaling but CD54-dependent cluster formation is not essential to resist PGE₂-mediated suppression in IL-15 activated NK cells.

CD25⁺/CD54⁺ NK cells display superior anti-tumor capacity

Given that the frequency of CD25⁺/CD54⁺ remained significantly higher upon exposure to PGE₂ in IL-15 activated NK cells, this population of NK cells was further examined for its anti-tumor activity. After 2 days of cytokine activation, NK cells were sorted for CD25 and CD54 (Fig EV3F). Regardless of activation with either IL-2 or IL-15, CD25⁻/CD54⁻ NK cells were unable to kill target cells even in the absence of PGE₂ (Fig 4A). In contrast, CD25⁺/CD54⁺ purified from either IL-2 or IL-15 activated NK cells displayed high cytotoxic activity. Further investigation of the CD25⁺/CD54⁺ NK cells revealed higher levels of perforin, TRAIL, CD107a, and IFN γ while granzyme B remained at similar levels compared with CD25⁻/CD54⁻ NK cells, suggesting that the superior cytotoxicity of CD25⁺/CD54⁺ NK cells are mediated through perforin and TRAIL (Fig 4B–F).

To dissect the underlying mechanisms for the superior cytolytic activity of CD25⁺/CD54⁺ NK cells, NK cells were activated with IL-15 and thereafter analyzed for the phosphorylation of pS6 and expression of PDE4A. CD25⁺/CD54⁺ NK cells showed significant increase in pS6 and PDE4A compared with CD25⁻/CD54⁻ NK cells (Figs 4G and H, and EV3G). In addition, immunofluorescence staining revealed a substantially lower expression of PDE4A in CD25⁻/CD54⁻ NK cells compared with CD25⁺/CD54⁺ NK cells (Fig 4I).

To test if CD25⁺/CD54⁺ NK cells are resistant to PGE₂-mediated suppression, NK cells were first activated by IL-15 for 2 days, thereafter sorted as CD25⁺/CD54⁺ or CD25⁻/CD54⁻ NK cells, and then exposed to PGE₂ during the killing assay. CD25⁻/CD54⁻ NK cells showed significantly reduced ability to kill K562 target cells regardless of PGE₂ exposure or not. In contrast, CD25⁺/CD54⁺ showed significantly higher ability to kill K562 target cells even in the presence of PGE₂ (Fig 4J).

Since previous studies have highlighted that mTOR activity is linked with increased metabolic activity in NK cells, the mitochondrial mass and mitochondrial membrane potential was analyzed in CD25⁺/CD54⁺ and CD25⁻/CD54⁻ purified NK cells (Marcais *et al*, 2017; Zheng *et al*, 2019b). Flow cytometry and confocal imaging analysis revealed a higher mitochondrial mass (MitoTracker Green) and mitochondria membrane potential (MitoTracker Red FM) in CD25⁺/CD54⁺ NK cells compared with CD25⁻/CD54⁻ NK cells (Fig 4K and L).

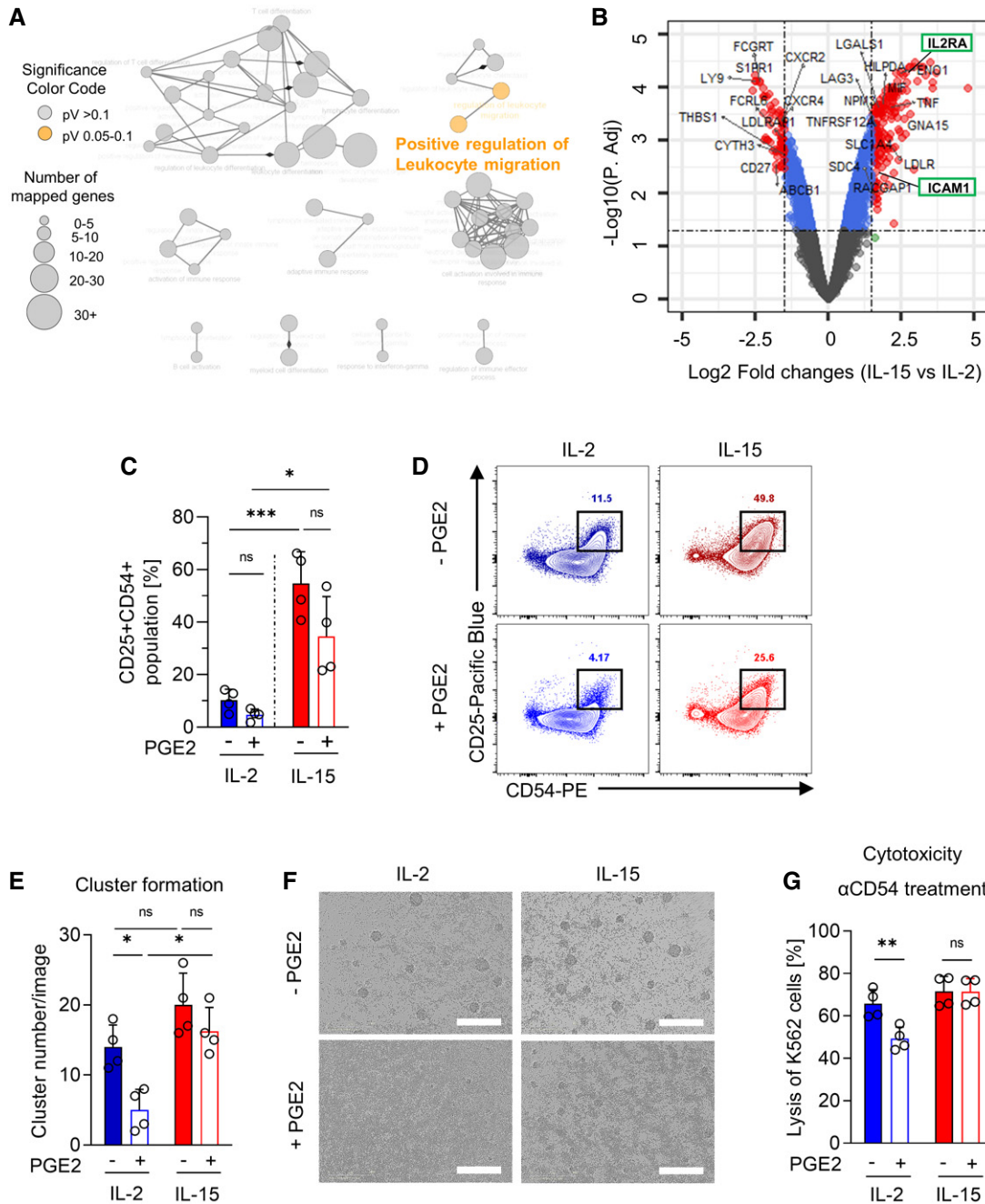


Figure 3. IL-15 induces phenotypical changes and supports the formation of cell clustering.

A Gene ontology enrichment analysis showing immune system process (GO:0002376) pathways for genes with > 1.5 fold change expression between IL-15 and IL-2. The color of the nodes is determined by the significance of the enriched term by two-sided hypergeometric test with Bonferroni's step-down method for P value correction.

B Volcano plot showing genes compared after 2 days cytokine-activated NK cells. Genes with significant changes (P value < 0.05) and > 1.5 log₂ fold change between IL-2 and IL-15 activated NK cells are labeled in red. Genes belonging to cell surface (GO:0009986) are annotated with gene name.

C Quantification of CD25⁺ CD54⁺ population changes after 2 days treatment (n = 4, biological replicates).

D Representative flow cytometry graphs for CD25 and CD54 staining in IL-2 and IL-15 NK cells in the presence or absence of PGE₂.

E Quantification of the number of cell clusters. NK cell clusters were defined as cell aggregates occupying an area at least 2,000 μm² and an eccentricity of < 0.8. (n = 4, biological replicates).

F Representative phase contrast image of IL-2 and IL-15 activated NK cells in the presence or absence of PGE₂. Scale bar 50 μm.

G Chromium-release cytotoxicity assay by 2-day cytokine-activated NK cells in the presence or absence of PGE₂ (1 μM) and anti-CD54 (20 μg/ml; n = 4, biological replicates), E:T ratio = 5:1.

Data information: Data were analyzed using a paired parametric t-test (*P < 0.05, **P < 0.01, ***P < 0.001). Each circle represents an individual experiment. Error bars are depicted as standard deviation.

These results demonstrate that CD25⁺/CD54⁺ NK cells resist PGE₂-mediated suppression and have higher levels of pS6, PDE4A and increased mitochondrial activity compared with CD25⁻/CD54⁻ NK cells.

PTGES affects the prognostic value of NK cells in patients with lung adenocarcinoma

To investigate any potential relationship between infiltration of NK cells and the presence of PGE₂ on prognosis in patients with cancer, gene expression analysis of prostaglandin E synthase (*PTGES*) was performed across 33 TCGA data cohorts (Appendix Fig S1B). In lung adenocarcinoma (LUAD), the expression of *PTGES* was significantly higher in tumor tissue compared with normal tissue (Fig 5A). A high *PTGES* expression showed a significant negative correlation with overall survival and disease-free survival in lung adenocarcinoma (Fig 5B). Using specific gene expression signature to identify NK cells, as defined by Bottcher *et al* (2018), we found that in contrary to *PTGES* expression, NK cells level was significantly lower in tumor tissue compared with normal tissue (Fig 5C). Between the different stages, stage I LUAD showed significantly higher NK cell gene expression signature compared with patients with stage III LUAD. Notably, the expression of *IL-15* was higher in patients with a high NK cell gene expression (Fig 5D).

We next sought to investigate the prognostic value of NK cells in different disease stages in LUAD. In stage I lung adenocarcinoma, a high NK cell gene signature positively correlated with improved overall survival (Fig 5E). However, NK cell gene signature was not associated with survival rate in late stage (II–IV) lung adenocarcinoma (Fig EV4A). To investigate whether NK cell gene signature and the expression of *PTGES* have an impact on survival in lung adenocarcinoma, samples were divided based on high and low *PTGES* expression. While NK cell gene signature was not associated with improved survival in patients with low expression of *PTGES* (HR = 1.337), a high NK cell gene signature correlated with improved survival in patients with high *PTGES* expression (HR = 1.517; Figs 5F and EV4B). Taken together, these results show that *PTGES* is a factor for poor prognosis and it affects the prognostic value of NK cells in patients with lung adenocarcinoma. Furthermore, NK cell gene expression signature has a prognostic value in stage I lung adenocarcinoma.

CD54-positive NK cells infiltrate lung adenocarcinoma tumors

Given the prognostic value of NK cell infiltration in patients with *PTGES* high lung adenocarcinoma, we sought to confirm these results using an *in vitro* lung cancer model. Purified NK cells were co-cultured with the lung cancer cell line A549 in the presence or absence of PGE₂. The ability of IL-2 activated NK cells to kill A549 cells was significantly delayed compared with IL-15 activated NK cells. Although the presence of PGE₂ reduced the killing by both IL-2 and IL-15 activated NK cells, the ability of IL-15 but not IL-2 NK cells to kill A549 cells was restored at 12 h (Fig 6A). Similar to killing of K562 cells, CD25⁺/CD54⁺ NK cells maintained their killing of A549 in the presence of PGE₂ (Fig 6B). While A549 cells cultured as 3D-spheroids produce PGE₂, monolayer cultured A549 cells did not produce any detectable PGE₂ (Fig EV4C). When added to A549 spheroids, CD25⁺/CD54⁺ NK cells showed increased infiltration

compared with CD25⁻/CD54⁻ NK cells (Figs 6C and D, and EV4D, Movies EV1 and EV2). The total number of both tumor-infiltrating and tumor-non-infiltrating NK cells was similar between CD25⁺/CD54⁺ and CD25⁻/CD54⁻ NK cells, confirming an equal NK cell seeding throughout the assay (Fig 6E). To confirm these results, tumor spheroids were harvested and analyzed for the presence of NK cells by flow cytometry. Indeed, CD25⁺/CD54⁺ NK cells were present at higher frequencies within the spheroids compared with CD25⁻/CD54⁻ NK cells (Fig 6F and G).

To further substantiate if CD25⁺/CD54⁺ NK cells infiltrate tumors at higher frequencies compared with CD25⁻/CD54⁻ NK cells site, a xenograft zebrafish model was developed. A549 tumor burden was significantly reduced in animals treated with CD25⁺/CD54⁺ NK cells. In contrast, injection of CD25⁻/CD54⁻ did not significantly reduce the tumor burden (Fig 6H and L). In addition, CD25⁺/CD54⁺ NK cells infiltrated A549 tumors to a significantly higher degree compared with CD25⁻/CD54⁻ NK cells (Fig 6I and K). Furthermore, the distance between the tumor and CD25⁺/CD54⁺ NK cells was significantly lower than that of the distance between the tumor to CD25⁻/CD54⁻ NK cells (Fig 6J). The overall injected CD25⁻/CD54⁻ NK cells remained at the same frequencies as CD25⁺/CD54⁺ NK cells (Fig 6M).

Finally, infiltration of NK cells was analyzed in a cohort of lung adenocarcinoma patients (*n* = 10). Comparing the center of the tumor, invasive margin, and normal adjacent tissue, NK cell frequency was significantly higher in the invasive margin and normal adjacent tissue compared with the center of the tumor. While the median frequency of CD25-positive NK cells was 5.31%, the frequency of CD54-positive NK cells ranged between 12.5–64.3%. The frequency of CD54-positive NK cells was significantly higher in the central tumor region compared with the invasive margin and normal adjacent tissue (Fig 6N). Taken together, these results show that NK cells expressing CD25 and CD54 have superior capacity to kill and infiltrate lung cancer cells in the presence of PGE₂ and that NK cells expressing CD54 are more abundant within central lung cancer tissue.

Discussion

Intratumoral NK cell frequency correlates with improved prognosis in several different cancers (Barry *et al*, 2018; Lee *et al*, 2019; Souza-Fonseca-Guimaraes *et al*, 2019). However, suppressive factors produced within the tumor microenvironment including PGE₂ limit the activation of NK cells (Park *et al*, 2018). Here we show that NK cells activated by IL-2 are suppressed by PGE₂, whereas IL-15 activated NK cells are less sensitive to suppression by PGE₂. The reduced susceptibility to PGE₂ was dependent on the expression of the cyclic nucleotide phosphodiesterase family member PDE4A.

The expression of PDE4 family members has been linked to tumor progression and metastatic dissemination in lung cancer and hepatocellular carcinoma (Pullamsetti *et al*, 2013; Peng *et al*, 2018). PDE4A is also expressed in human inflammatory cells including T cells and monocytes where it terminates the activity of cAMP by hydrolyzing it into AMP (Manning *et al*, 1999). Intracellular cAMP acts as a potent immunosuppressive signaling molecule in T and NK cells and is upregulated by multiple factors including PGE₂ (Harris *et al*, 2002). Recently, overexpression of PDE4A in T cells was

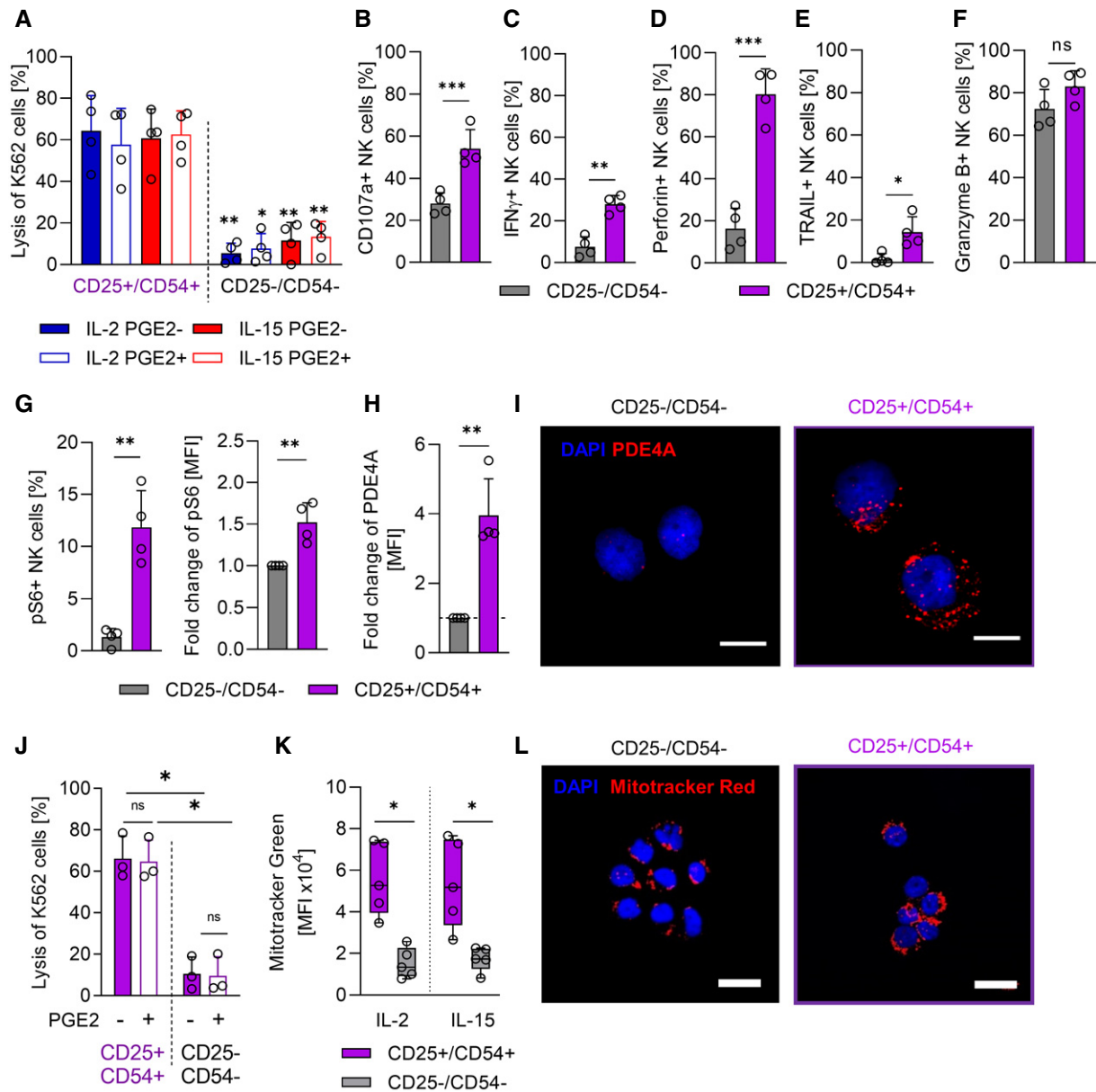


Figure 4. CD25⁺/CD54⁺ NK cells display high cytolytic capacity in the presence of PGE₂.

- A** NK cells were stimulated with either IL-2 or IL-15 in the presence or absence of PGE₂ for 2 days and thereafter purified as CD25⁺/CD54⁺ and CD25⁻/CD54⁻ and tested in a ⁵¹Cr-release assay against K562. (E: T = 5:1, *n* = 4, biological replicates). Stars indicate significant *P*-values comparing CD25⁺/CD54⁺ vs CD25⁻/CD54⁻ NK cells for each condition.
- B–F** NK cells were stimulated with IL-15 and purified as CD25⁺/CD54⁺ and CD25⁻/CD54⁻ and co-cultures with K562 cells (5:1 ratio) for 6 h and analyzed for the expression of (B) CD107a, (C) IFN γ , (D) Perforin, (E) TRAIL and (F) Granzyme B were by flow cytometry (*n* = 4, biological replicates).
- G** Flow cytometry analysis of levels (Left = % frequency, right = fold change of mean fluorescence intensity) of phosphorylated S6 (S235/236) in CD25⁺/CD54⁺ and CD25⁻/CD54⁻ IL-15 activated NK cells (*n* = 4, biological replicates).
- H** Flow cytometry analysis of PDE4A expression in CD25⁺/CD54⁺ and CD25⁻/CD54⁻ IL-15 activated NK cells (*n* = 4, biological replicates).
- I** Representative image of PDE4A expression in CD25⁺/CD54⁺ and CD25⁻/CD54⁻ IL-15 activated NK cells. Scale bar: 10 μ m.
- J** NK cells were first stimulated with IL-15 for 2 days in the absence of PGE₂, then purified as CD25⁺/CD54⁺ or CD25⁻/CD54⁻ NK cells and tested in a ⁵¹Cr-release cytotoxicity assay against K562 cells at an E:T ratio of 5:1 in the presence (filled bars) or absence (open bars) of PGE₂ (1 μ M; *n* = 3, biological replicates).
- K** Mitochondria mass from purified CD25⁺/CD54⁺ and CD25⁻/CD54⁻ NK cells measured by flow cytometry (*n* = 5, biological replicates).
- L** Representative image of MitoTracker Red FM in CD25⁺/CD54⁺ NK cells and CD25⁻/CD54⁻ NK cells. Scale bar: 20 μ m.

Data information: Data were analyzed using a paired parametric *t*-test (**P* < 0.05, ***P* < 0.01, ****P* < 0.001). Each circle represents an individual experiment. Error bars are depicted as standard deviation. Box and whiskers plots (K): box extends from 25th to 75th percentile, the center line indicates the median and whiskers indicate min and max values.

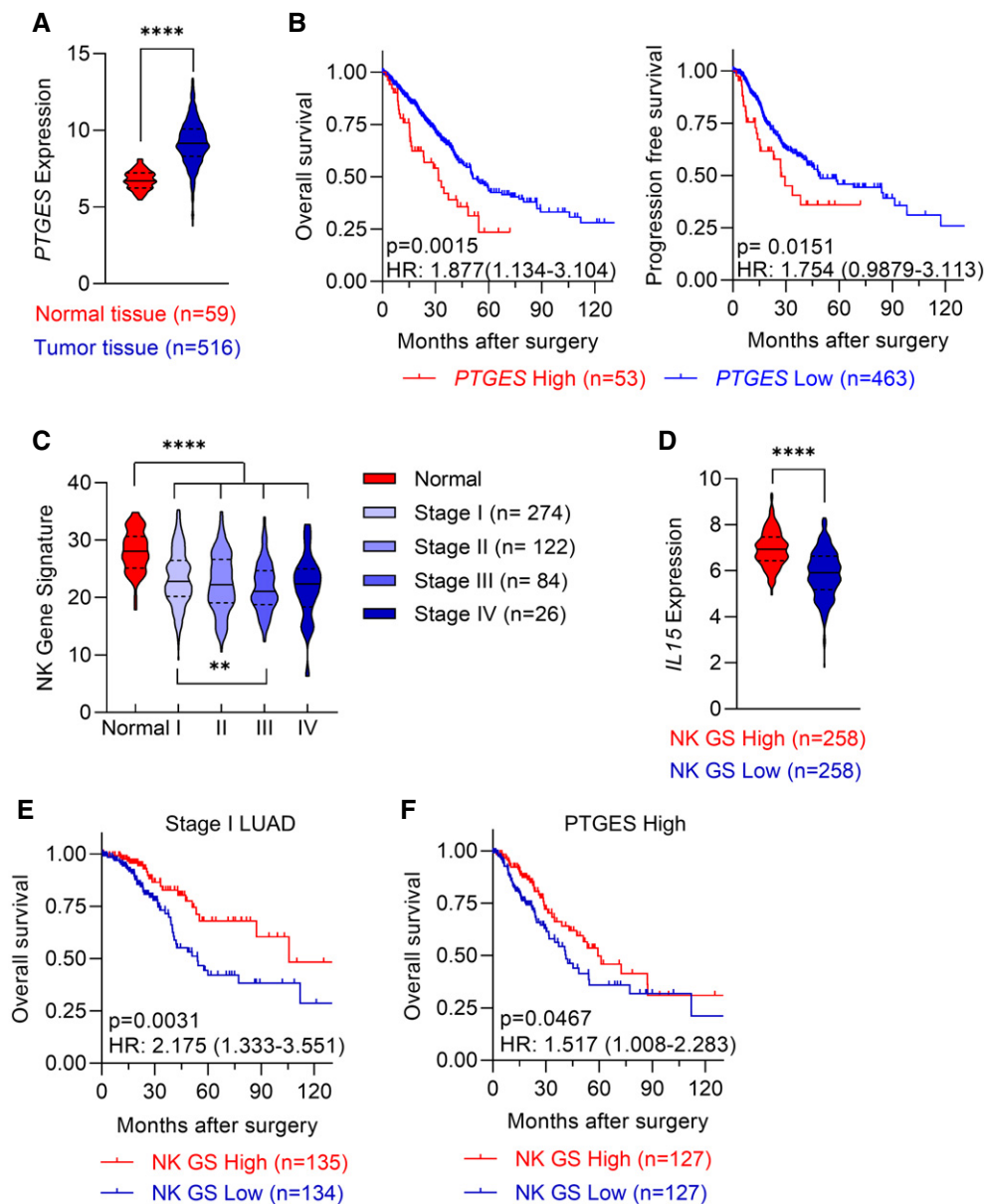


Figure 5. *PTGES* affects the prognostic value of NK cells in patients with lung adenocarcinoma.

A Expression of *PTGES* in normal and tumor tissue.

B Kaplan–Meier analysis of overall (left) and progression-free (right) survival in patients with lung adenocarcinoma with high *PTGES* (top 10%) and low *PTGES* (bottom 90%) expression.

C NK cell gene signature in normal and tumor tissues based on a TCGA lung adenocarcinoma cohort and quantification of NK cell gene signature in patients with different stages of lung adenocarcinoma.

D IL15 gene expression analysis in high and low NK gene signature (NK GS).

E Overall survival in patients with stage I ($n = 269$) lung adenocarcinoma with high (top 50%) and low (bottom 50%) NK cell gene expression signature expression.

F Overall survival in patients with high (top 50%) *PTGES* expression in relation to high (top 50%) and low (bottom 50%) NK cell gene expression signature.

Data information: Panels A, C, D were analyzed using an unpaired parametric *t*-test (**** $P < 0.0001$). Log-rank (Mantel–Cox) test was used to test for significance and log-rank *P*-values are displayed in Kaplan–Meier analysis graph. ** $P < 0.01$, **** $P < 0.0001$. LUAD: Lung adenocarcinoma. HR is calculated at 95% CI. The violin plots in A, C and D show the median (solid line) and the 25th and 75th percentile (dashed line).

proposed as an immune checkpoint inhibitor against cAMP-mediated immunosuppression *in vitro* (Schmetterer *et al*, 2019). However, the role of PDE4A in regulating the levels of cAMP in

human NK cells is unknown. Here, we first show that IL-15 increases the expression of PDE4A and inhibition of PDE4A increases the levels of cAMP.

Exposure to IL-15 activates mTOR signaling in human NK cells (Marcais *et al*, 2014; Mao *et al*, 2016; Wang *et al*, 2018). While inhibition of PDE4D, another PDE4 member capable of hydrolyzing cAMP into AMP, can suppress mTOR activity in colorectal cancer cells, it is unknown if PDE4A cross-talk with mTOR in human NK cells (Kim *et al*, 2019). A recent study showed that increased cAMP signaling activates protein kinase A (PKA) and inhibits mTORC1 (Jewell *et al*, 2019). Here we demonstrate that inhibition of mTOR reduces the expression of PDE4A. Likewise, inhibition of PDE4A reduces the activation of mTOR signaling. Thus, there is a reciprocal cross-talk between mTOR and PDE4A in human NK cells.

The 5' AMP-activated protein kinase (AMPK) acts as a sensor of cellular energy status and is activated under conditions of low intracellular ATP. Given that AMPK can inhibit mTOR and that PDE4 was recently shown to regulate AMPK-dependent autophagy, it is plausible that AMPK can also affect the expression of PDE4A and mTOR activity in NK cells (Gwinn *et al*, 2008; Zhong *et al*, 2019). Upon exposure to PGE₂, pAMPK levels were significantly upregulated in both IL-2 and IL-15 stimulated NK cells. Furthermore, the expression of CD54 and frequency of CD25⁺/CD54⁺ was significantly reduced upon inhibition of AMPK using compound C. In addition, pAMPK levels were not affected upon inhibition of mTOR, whereas the expression of PDE4A and pS6 were significantly reduced upon inhibition of AMPK (Appendix Fig S2). Taken together, these results indicate AMPK does play a role to regulate NK cell expression of CD54, PDE4A, and mTOR in NK cells.

Upregulation of PDE4A was only observed upon IL-15 stimulation but not upon stimulation with IL-2. We previously demonstrated that IL-15 is superior to IL-2 to increase mTOR activity and that priming with IL-15 increases differential translation compared with NK cells primed with IL-2 (Mao *et al*, 2016). Although IL-2 and IL-15 both rely on the JAK/STAT signaling pathway, stimulation with IL-15 resulted in a higher phosphorylation of STAT5. Furthermore, STAT5 was identified as a putative transcription factor binding to PDE4A thus strengthening our results that PDE4A expression is regulated via IL15/JAK/STAT5 signaling.

Compared with IL-2, activation with IL-15 changes the expression of several cell surface receptors. Similar to other studies, we previously showed that the expression of CD25 is significantly higher upon activation with IL-15 compared with IL-2 (Dybkaer *et al*, 2007; Bezman *et al*, 2012; Pradier *et al*, 2014; Mao *et al*, 2016). Our present study confirms these results and also shows that the expression of CD54 is significantly higher on NK cells upon IL-15 stimulation compared with IL-2 stimulation.

CD54 is an adhesion molecule expressed by hematopoietic and non-hematopoietic cells and can be upregulated on lymphocytes following activation (Roy *et al*, 2001; Harjunpaa *et al*, 2019). Ligation of adhesion molecules is a hallmark for lymphocyte activation and an initial step for immune synapse formation to drive the cancer-NK cell immunity cycle (Huntington *et al*, 2020). The expression of CD54 is well-studied on myeloid cells but few studies have focused on studying CD54 and its role in human NK cells. Early studies have shown that IL-15 upregulates the expression of CD54 on human cord-blood derived NK cells and on NK cell lines (Lin & Yan, 2000; Zhang *et al*, 2004). NK cells expressing CD54 following IL-15 stimulation show a higher capacity to adhere to cell culture plastics (Sun *et al*, 2003). A recent study by Ni *et al* (2020) showed that cytokine-activated IFN γ -producing NK cells express higher levels of several activating receptors as well as CD54. Basingab *et al* (2016) showed that the overexpression of CD54 on tumor cells counteracts immune-suppression by PGE₂ to restore T-cell activity. Here, we found that IL-15-induced CD54 resulted in a higher capacity to form cell clusters even in the presence of PGE₂. However, blocking the CD54 receptor did not change susceptibility of NK cell to PGE₂-mediated suppression. Through further analysis of NK cells expressing CD25 and CD54 following activation with IL-15, only the population of cells expressing both receptors showed increased S6 phosphorylation and PDE4A expression, and an increased capacity to resist PGE₂-mediated suppression *in vitro*. We hypothesize that CD25 is essential to preserve NK cell function under PGE₂-cAMP pressure; however, we were unable to test this hypothesis due to the low

Figure 6. CD54-positive NK cells infiltrate lung adenocarcinoma tumors.

- A Real-time image-based killing of A549 cells by NK cells isolated from two individual healthy donors at an E:T ratio of 10:1.
- B NK cells were stimulated with IL-2 or IL-15 in the presence or absence of PGE₂ and then purified as CD25⁺/CD54⁺ or CD25⁻/CD54⁻ cells and tested for cytotoxicity against A549 tumor cell in a 51Cr-release assay. E:T ratio = 5:1 (*n* = 4, biological replicates). Stars indicate significant *P*-values comparing CD25⁺/CD54⁺ vs CD25⁻/CD54⁻.
- C Representative image of NK cell infiltration (red) into A549 tumor spheroids at the time of addition of NK cells and at 20 h after the addition of NK cells, scale bar: 400 μ m.
- D, E Incubate quantification of (D) total and (E) tumor-infiltrating CD25⁺/CD54⁺ and CD25⁻/CD54⁻ NK cells. RCU, Red Calibrated Unit (*n* = 4, biological replicates).
- F, G Flow cytometry quantification of (F) tumor-infiltrating and (G) non-infiltrating NK cells. Results are depicted as total NK cells among CD45-positive live cells. (*n* = 4, biological replicates).
- H 48 h dpi zebrafish injected with A549, A549⁺CD25⁺/CD54⁺, or A549⁺CD25⁻/CD54⁻ NK cells after 24 h. Fluorescent image was taken by Leica epi-fluorescent stereomicroscope. Scale bar: 500 μ m. The tumor injection area (perivitelline space) is depicted with a dashed line.
- I 3D view of tumor injection area 24 h post-tumor inoculation (left). Scale bar = 50 μ m. The tumor injection area (perivitelline space) is depicted with a dashed line. Magnified view for tumor area (right). The A549-td tumor cells are annotated with a purple translucent mask and NK cells are color-coded based on the distance to the tumor area (near-far: blue-red). Scale bar = 10 μ m.
- J The distance between NK cells and tumor area in CD25⁻/CD54⁻ and CD25⁺/CD54⁺ NK cell treated fish (*n* = 5, biological replicates).
- K Frequency of tumor-infiltrating NK cells in CD25⁻/CD54⁻ and CD25⁺/CD54⁺ NK cell treated fish (*n* = 5, biological replicates).
- L, M Quantification of (L) tumor cell and (M) NK cell counts 24 h after injection of NK cells by Imaris (*n* = 5, biological replicates).
- N Frequency of tissue-infiltrating total NK cells (CD56⁺/CD3⁻; left) and CD54-positive NK cells (right) among CD45-positive live cells (*n* = 10, biological replicates).

Data information: Data were analyzed using a paired parametric *t*-test (**P* < 0.05, ***P* < 0.01, ****P* < 0.001, *****P* < 0.0001). Each circle represents an individual experiment. Error bars are depicted as standard deviation. The violin plots in J and K show the median (solid line) and the 25th and 75th percentile (dashed line).

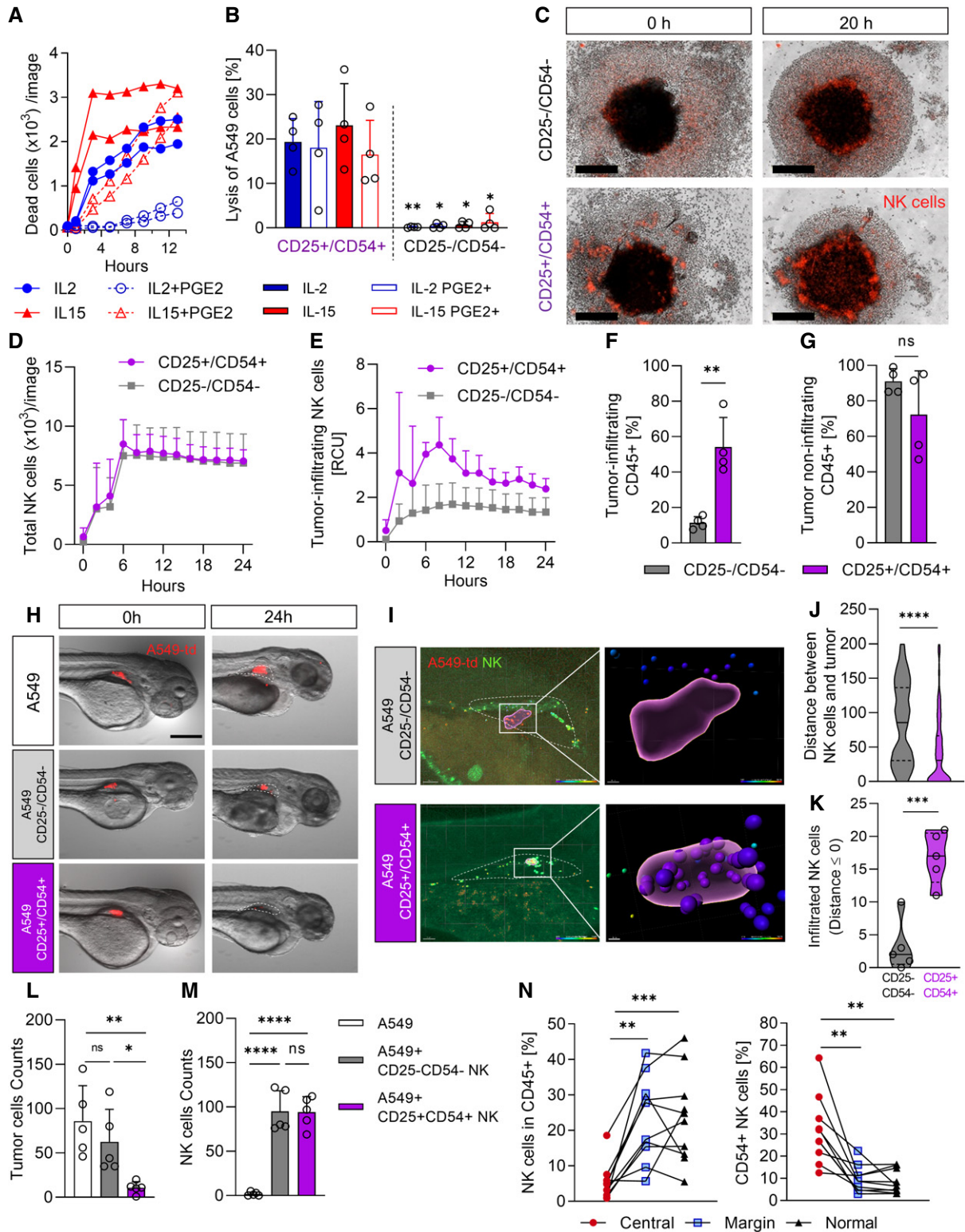


Figure 6.

frequency of CD25 single positive NK cells following activation with IL-15.

The role of PGE₂ has previously been studied in lung cancer where it can synergize with IL-17 to form an M2 macrophage-dominant

tumor microenvironment (Liu *et al*, 2012). In an experimental lung cancer model, Ogawa *et al* (2014) found that aspirin reduces lung cancer metastasis to regional lymph nodes. From the analysis of TCGA dataset, we found a higher expression of *PTGES* in lung

cancer tissue compared with normal tissue and that *PTGES* is a poor prognostic factor in lung adenocarcinoma. Furthermore, NK cell gene expression signature correlated with improved prognosis in early but not late stage lung adenocarcinoma, suggesting that NK cells play a role in the immune surveillance in early stage lung adenocarcinoma.

Despite high expression of *PTGES* in tumors, NK cell gene expression was still detected. To investigate if tumors with high and low NK cell gene expression differ in tumors with a high *PTGES* expression, we performed gene set enrichment analysis. Tumors with high *PTGES* and high NK cell gene expression showed enriched expression of inflammatory-related pathways including T-cell activation, T-cell receptor signaling pathway, activation of innate immune response, and positive regulation of cytokine production (Appendix Fig S3). These results indicate that *PTGES* high tumors with high NK cell gene expression are in general more inflamed than *PTGES* high tumors with a low NK cell gene expression. Thus, inflammatory pathways could potentially increase the persistence of NK cell despite high levels of *PTGES*.

Notably, NK cell high gene expression signature correlated with improved prognosis and significant improved overall survival only in patients with *PTGES* high tumors. These observations might be explained by an existing NK cell-dependent immune selective pressure in the *PTGES* high tumors. Zelenay *et al* (2015) showed that genetic ablation of COX through *PTGS2* knock-out shifts the tumor inflammatory profile, where an increase in *Cd25*, *Ifng*, and *Gzmb* is observed, thereby impairing the tumor growth. Here, we show that the CD25⁺CD54⁺ subpopulation of NK cells resists such immune escape mechanism by being unresponsive to suppression by PGE₂.

Natural killer cells generally showed a poor infiltration in central lung cancer tissue compared with peripheral lung cancer tissue, but NK cells expressing CD54 showed a preferential infiltration into the central tumor region. Similarly, NK cells expressing CD25 and CD54 showed significantly higher ability to infiltrate lung adenocarcinoma spheroids *in vitro*. In addition, these NK cells showed increased ability to kill lung adenocarcinoma cells *in vitro*. These data suggest that the expression of CD54 is required for NK cells to infiltrate lung adenocarcinoma tissue.

The zebrafish is a recent addition to animal models of human cancer (Fior *et al*, 2017; Hason & Bartunek, 2019; Yan *et al*, 2019). With optically clear zebrafish model, visualization of single-cell phenotypes is applicable. Here we report a model based on infusion of NK cells to monitor tumor cells growth *in vivo* in zebrafish. Consistent with our *in vitro* results, CD25⁺CD54⁺ NK cells show superior ability to infiltrate and kill lung adenocarcinoma tumors.

In summary, we investigated if modulation of the cytokine milieu represents a strategy to render NK cells less susceptible to tumor-induced immunosuppression to increase their intratumoral persistence. This approach was recently shown by Fujii *et al* (2018) who demonstrated that IL-15 protects and rescues NK cell cytotoxicity from TGFβ-mediated immunosuppression. Here we uncover a unique mechanism of IL-15 to activate NK cells to resist PGE₂-mediated suppression. Mechanistically, IL-15 enriches a subset of CD25⁺/CD54⁺ NK cells with superior mTOR activity and PDE4A expression. Therefore, approaches to selectively expand CD25⁺CD54⁺ NK cells for adoptive cell therapy represent a potential therapeutic strategy for patients with tumors producing high levels of PGE₂.

Materials and Methods

Human specimen

All human specimens were collected from patients with primary diagnosis of Non-small-cell lung cancer (NSCLC). Written informed consent was signed by all the patients for sample acquisition for research purposes. This study was conducted under the approval of the Ethics Committee of the Second Affiliated Hospital of Zhejiang University (IR2019001101). Fresh specimens ($n = 10$) were obtained from patients undergoing lung resection surgery. All patients were diagnosed with adenocarcinoma and received no previous cancer treatment before the resection. Pathology diagnosis was based on routine H&E staining and cytological assessments. Central tumor tissue, adjacent tumor tissue, and non-adjacent normal lung tissue were collected within 2 h after resection and immediately processed for flow cytometry analysis (Appendix Fig S1D). The non-adjacent normal lung tissues were taken as distant as possible from the tumor and were reviewed by a pathologist. The clinical and pathologic characteristics of all patients included in this study are summarized in Appendix Table S1.

Cell culture

Peripheral blood mononuclear cells (PBMC) were isolated from buffy coat by Ficoll gradient centrifugation (GE healthcare) and washed three times in PBS, followed by red-cell lysis by ACK buffer (Thermo Fisher). NK cells were purified from PBMC using negative selection microbeads (NK cell isolation kit, human, Miltenyi biotech) according to the manufacturer's protocol. The purity of isolated NK cells was above 95% as assessed by flow cytometry staining for CD56 and CD3. Isolated NK cells were seeded in 48-well flat-bottom plate (TPP techno) in X-vivo 20 medium (Lonza) supplemented with 10% heat-inactivated human AB serum and 300 IU/ml of IL-2 or 21 ng/ml IL-15. Where indicated, NK cells were cultured in the presence of 1 μM PGE₂ (Sigma Aldrich), 1 μM Torin-1 (SelleckChem), or 1 μM PDE4 inhibitor, (Roflumilast, SelleckChem). The NSCLC cell line A549, A549-tdtomato cell line and chronic myelogenous leukemia cell line K562 were maintained in RPMI1640 medium (Life Technologies) supplemented with 10% heat-inactivated FBS (Life Technologies) and 1% antibiotics (penicillin, streptomycin).

Cytotoxicity assays

Natural killer cell cytotoxicity was measured by chromium-release assay (4 h) against K562 and A549 cells at a 5-to-1 effector-to-target ratio, as previous described (Mao *et al*, 2016). For real-time killing, A549 cells were labeled with IncuCyte® NucLight Rapid Red Reagent (Essen BioScience) at a dilution of 1:1,000, then seeded at 5,000 cells per well into a 96-well flat-bottom plate in RPMI medium supplemented with 10% FBS (Invitrogen) and cultured at 37°C overnight to attach. NK cells were plated at 25,000 cells per well in complete RPMI medium, with or without PGE₂. IncuCyte® Caspase-3/7 Green Apoptosis Assay Reagent (Essen Bioscience) was added to each well at a dilution of 1:1,000. The assay plate was monitored, and four images were acquired per well every hour. Average numbers of dead tumor cells were determined at each time point

using the IncuCyte live-cell analysis software. Where indicated, anti-CD54 antibody (20 µg/ml) was added to assays.

Real-time imaging-based cluster assay

Live content imaging and analysis was performed with an IncuCyte S3 system (Essen Bioscience, Sartorius). In brief, images of cytokine-activated NK cells were taken with a 10× objective lens every 2 h from initial cell seeding. IncuCyte S3 software was used to automatically score and quantify cluster formation. Clusters were defined as cell aggregates occupying an area at least 2,000 µm² and an eccentricity (non-circularity) of < 0.8.

Quantitative RT-PCR

Total RNA was extracted from 0.5 million cultured NK cells using the RNeasy Micro Kit (Qiagen). cDNA was synthesized according to the manufacturer's instructions of QuantiTect Reverse Transcription Kit (Qiagen). Quantitative real-time PCR was performed using Power SYBR Green PCR Master Mix (Thermo Fisher) and detected on the CFX96 Touch Real-Time PCR Detection System (Bio-Rad). The expression levels of each gene were determined according to the comparative Ct method and normalized to housekeeping gene TBP. The sequences of used primers are described in the Appendix Table S2.

CistromeDB toolkit

Data type used in CistromeDB as “Transcription factor, chromatin regulator”, the interval of PDE4A (chr19:10,416,773–10,469,631/hg38) was submitted via CistromeDB (<http://dbtoolkit.cistrome.org/>) (Zheng *et al*, 2019a). Results were downloaded from the website and plotted using GraphPad Prism (GraphPad).

Flow cytometry

Detailed information of antibodies used in this study is summarized in Appendix Table S3. Briefly, 1–2 × 10⁵ cells were harvested in Falcon® Round-Bottom Polystyrene Tubes (BD) and washed twice with FACS buffer (PBS with 2% FBS). Next, cells were resuspended in 20 µl PBS containing the appropriate antibody cocktails for extracellular antigens and incubated at 4°C for 30 min. Cells were acquired on a Novocyte flow cytometer (ACEA biosciences) and analyzed by Flowjo (BD). For intracellular staining, the stain-fix-perm procedure performed according to BD phosflow alternative protocol II as used. In brief, following staining for cell surface antigens, cells were fixed in BD phosflow fix buffer for 10 min, and wash twice with PBS. Then, cells were incubated on ice with BD phosflow perm buffer III for 30 min, followed by three times washing prior staining for intracellular antigens.

For degranulation and intracellular staining for perforin and IFN γ , NK cells were incubated with an equal amount of K562 cells for 4 h in medium containing CD107a and CD56 antibodies. Golgiplug (BD) and Golgistop (BD) were added in order to accumulate cytokine production during incubation with K562. Intracellular staining for IFN- γ and Perforin was performed as previously described (Neo *et al*, 2020).

For mitochondria staining, sorted cells were stained with MitoTracker Green FM in accordance with manufacture's guidelines

(Thermo Fisher). Following three washing steps with FACS buffer, cells were acquired on a Novocyte flow cytometer (ACEA biosciences) and analyzed by Flowjo (BD) and SPICE 6.0 (Roederer *et al*, 2011). Gating strategy for NK cells is shown in Appendix Fig S1A.

For analysis of spheroid cultures, 5,000 A549 cells were seeded in Nunclon sphera 96-well Round (U) bottom plate (Thermo Fisher) for 7 days. NK cells were labeled with IncuCyte® NuLight Rapid Red Reagent (Essen BioScience) and added at 25,000 cells to each well. Following 24 h co-culture, spheroids were gently resuspended in 1 ml PBS and left to sediment to the bottom of a 5-ml Eppendorf tube. This washing step was repeated twice. After each washing step, supernatants were collected as non-tumor-infiltrating NK cells. Spheroids containing tumor-infiltrating NK cells were harvested and trypsinized to obtain a single-cell suspension and thereafter analyzed by flow cytometry. Single-cell suspensions of spheroids and non-tumor-infiltrating cells were stained with Live/Dead cell marker and anti-CD45 antibody to distinguish NK cells from tumor cells.

Gene ontology enrichment analysis

Analysis of differentially expressed genes between IL-2 and IL-15 primed NK cells was performed using a 1.5-fold change cutoff from a publicly available data set (Mao *et al*, 2016). Comparative GO analysis among different categories of genes was performed using the ClueGo (2.5.4) plugin in Cytoscape (3.7.1). Gene IDs were submitted to query the GO-immunology process database. The working ClueGo parameters were set as follows: Evidence code set to: All; Use Go Term Fusion; GO tree interval, level 2–5; GO term selection minimum number of genes 8; GO term connectivity threshold (Kappa score) 0.7; Significance test using Two-sided hypergeometric test with Bonferroni step-down method for *P* value correction. Gene ontology terms are presented as nodes and clustered together based on the term similarity. Node size is proportional to the *P* value for GO term enrichment with larger node sizes representing more significant GO term. The node color is set according to the relative enrichment of the GO term in each cluster, gray color indicates no significant difference in enrichment for the represented term. The leading GO terms were annotated with larger font text for easier visualization. For cerebral view, CluePedia (1.5.4) plugin was used. Color coded with enriched pathway with annotation for cellular location from extra cellular to nucleus.

Immunofluorescence microscopy and image analysis

For intracellular staining, cells were fixed and permeabilized using the Foxp3/Transcription Factor Staining Buffer Set in accordance with manufacture's guidelines (eBioscience). Then, cells were incubated with primary antibodies and fluorescence-conjugated secondary antibodies. The nucleus was stained by Fluoroshield™ with DAPI (Sigma). For mitochondria staining, sorted cells were stained with MitoTracker Red FM according to the manufacture's guidelines (Thermo Fisher). Slides of stained cells were prepared with the cytospin 2 (SHANDON). Immunofluorescent staining was analyzed using the confocal laser scanning microscope LSM 700 system (Zeiss).

Zebrafish xenografts were fixed in 4% formaldehyde and stored in methanol at –20°C. Xenografts were mounted with 80% glycerol

on μ -Dish 35 mm (ibidi) monitored by confocal laser scanning microscope LSM Airy 800 (Zeiss). Confocal image stacks were reconstructed and visualized as three dimensional (3D) volumes with Imaris software (version 9.5; Bitplane). The Imaris Spot detection algorithm was used as described by the manufacturer for semi-automatic identification and counting of fluorescently labeled NK cells and A549-tdTomato. Main parameters were absolute thresholding, an object size of 5 μ m diameter, mean fluorescent intensity cutoff is 250. Errors in the software detection results (both erroneous positive and negative objects) were corrected by manual inspection of the data sets to adjust parameters.

cAMP and PGE₂ detection assays

Cytokine-activated NK cells were stimulated with 1 μ M PGE₂ for 5 min and intracellular cAMP was measured by competitive immunoassay using a cAMP Parameter Assay Kit (R&D Life Sciences) according to the manufacturer's instruction. Following culture for 7 days, supernatants were harvested and assayed for PGE₂ content by ELISA (R&D Life Sciences).

Cell sorting

Natural killer cells were sorted after 2 days of cytokine activation in the absence or presence of PGE₂. Cells were harvested and stained with surface antibodies against CD56, CD16, CD25, CD54, and Live/Dead cell marker. Stained cells were then sorted using BD FACSAria™ Fusion.

TCGA datasets analysis

All data were retrieved from The Cancer Genome Atlas (TCGA) lung adenocarcinoma (LUAD) dataset (<https://portal.gdc.cancer.gov/projects/TCGA-LUAD>). For generation of gene expression, NK cell gene signatures, normalized expression values were log₂-transformed and ranked by the mean expression value of signature genes. The following genes were used for NK cell gene signature: Natural Cytotoxicity Receptor 1 [NCR1], [NCR3], Killer Cell Lectin Like Receptor B1 [KLRB1], [CD160], Perforin 1 [PRF1] (Bottcher *et al*, 2018)). Overall survival analysis for *PTGES* and NK cell gene expression signature selected genes was performed with top and bottom expression values as indicated in respective figure legends and plotted as Kaplan–Meier curves using GraphPad Prism (GraphPad).

GEPIA 2 (<http://gepia2.cancer-pku.cn/>) was used to compare *PTGES* gene expression across 33 TCGA databases (Tang *et al*, 2019). Significantly changed ($P < 0.01$, $|\log_2FC| > 1$) cohort names were labeled in red for Tumor > Normal and green for Normal > Tumor. For pathways analysis of *PTGES*^{hi}NK^{hi} vs *PTGES*^{hi}NK^{low}, the top 200 genes that were significantly changed (Fold changes > 2, $P < 0.05$) in *PTGES*^{hi}NK^{hi} compared with *PTGES*^{hi}NK^{low} were processed via R for Gene Set Enrichment Analysis (GSEA).

Zebrafish tumor model

Zebrafish embryos were raised at 28°C under standard experimental conditions. Zebrafish embryos at the age of 24 hpf (hours post-fertilization) were incubated in water containing 0.2 mmol/l 1-phenyl-2-thio-urea (PTU, Sigma). At 48-hpf, zebrafish embryos

were dechorionated with a pair of sharp-tip forceps and anesthetized with 0.04 mg/ml of tricaine (MS-222, Sigma). Anesthetized embryos were subjected for microinjection. Sorted NK cells were labeled *in vitro* with 2 μ M of Carboxyfluorescein succinimidyl ester (CFSE) and mixed with A549-tdTomato cells (1:1 ratio) and injected at 5 nl (approximately total 500 cells) into the perivitelline space (PVS) of each embryo by an Eppendorf microinjector (FemtoJet 5247, Eppendorf and Manipulator MM33-Right, Märzhäuser Wetzlar). Non-filamentous borosilicate glass capillaries were used for injection and the injected zebrafish embryos were immediately transferred into PTU aquarium water 33°C until the end of experiment. 24 h after injection, zebrafish embryos were monitored by confocal laser scanning microscope LSM 700 system (Zeiss). Appendix Fig S1C illustrates the workflow for zebrafish injection.

Statistical analysis

Unless otherwise stated, all results were collected from multiple experiments and figures were prepared in a Prism 8.0 (GraphPad version 8). Differences between experimental groups were analyzed by paired Student's *t*-test. For TCGA dataset analysis, two-tail unpaired *t*-test was used. The difference in overall survival was tested using log-rank tests. All results are presented as mean \pm SD and represented histogram or images were selected based on the average values, $P < 0.05$ was considered significant (* $P < 0.05$; ** $P < 0.01$; *** $P < 0.005$; **** $P < 0.0001$).

Ethics approval

This study was conducted under the approval of the Ethics Committee of the Second Affiliated Hospital of Zhejiang University (IR2019001101), China. Written informed consent was signed by all the patients for sample acquisition for research purposes. For *in vivo* studies, no ethical permit is required as zebrafish embryos younger than 5 days have been used only. Those embryos are excluded from the normative on animal testing by the EU directive 2010/63/EU.

Data availability

RNA sequencing data are available under GSE77808 (<https://www.ncbi.nlm.nih.gov/geo/query/acc.cgi?acc=GSE77808>).

Expanded View for this article is available online.

Acknowledgements

We thank Biomedicum Imaging Core (BIC) and Zebrafish core facility at Karolinska Institutet. We thank Maria Johansson and Juan Basile at the Biomedicum Flow Cytometry Core Facility, Karolinska Institutet. We thank Kristina Witt, Weiyinqi Cui, and Luisa Wohn for technical input. This work was supported by grants from the Swedish Cancer Society (#CAN 2015/421 and #CAN 2018/451), the Swedish Childhood Cancer Foundation (#PR PR2014-0093 and PR2017-0049), the Cancer Research Foundations of Radiumhemmet (161192 and 181183), The Swedish Society for Medical Research, SSMF(P17-0134), and the China Scholarship Council (Grant no. 201600160070).

Author contributions

ZC, YY, LT, and SYN, conducted experiments and analyzed data. HS, YC, JW, AKW, contributed to acquisition of data and methods development. KL, P-JJ, YC, KW, and EA, contributed to data analysis and interpretation, and essential reagents. AL, YM, DS, LLL, conceived the project, supervised the research, and wrote the manuscript with input and editing from all authors.

Conflict of interest

The authors declare that they have no conflict of interest.

References

- Bachanova V, Cooley S, Defor TE, Verneris MR, Zhang B, McKenna DH, Curtsinger J, Panoskaltis-Mortari A, Lewis D, Hippen K et al (2014) Clearance of acute myeloid leukemia by haploidentical natural killer cells is improved using IL-2 diphtheria toxin fusion protein. *Blood* 123: 3855–3863
- Balsamo M, Scordamaglia F, Pietra G, Manzini C, Cantoni C, Boitano M, Queirolo P, Vermi W, Facchetti F, Moretta A et al (2009) Melanoma-associated fibroblasts modulate NK cell phenotype and antitumor cytotoxicity. *Proc Natl Acad Sci USA* 106: 20847–20852
- Barrow AD, Colonna M (2017) Tailoring Natural Killer cell immunotherapy to the tumour microenvironment. *Semin Immunol* 31: 30–36
- Barry KC, Hsu J, Broz ML, Cueto FJ, Binnewies M, Combes AJ, Nelson AE, Loo K, Kumar R, Rosenblum MD et al (2018) A natural killer-dendritic cell axis defines checkpoint therapy-responsive tumor microenvironments. *Nat Med* 24: 1178–1191
- Basingab FS, Ahmadi M, Morgan DJ (2016) IFN γ -dependent interactions between ICAM-1 and LFA-1 counteract prostaglandin E₂-mediated inhibition of antitumor CTL responses. *Cancer Immunol Res* 4: 400–411
- Bezman NA, Kim CC, Sun JC, Min-Oo G, Hendricks DW, Kamimura Y, Best JA, Goldrath AW, Lanier LL, Immunological Genome Project C (2012) Molecular definition of the identity and activation of natural killer cells. *Nat Immunol* 13: 1000–1009
- Bjorklund AT, Carlsten M, Sohlberg E, Liu LL, Clancy T, Karimi M, Cooley S, Miller JS, Klimkowska M, Schaffer M et al (2018) Complete remission with reduction of high-risk clones following haploidentical NK-cell therapy against MDS and AML. *Clin Cancer Res* 24: 1834–1844
- Bottcher JP, Bonavita E, Chakravarty P, Bles H, Cabeza-Cabrerizo M, Sammicheli S, Rogers NC, Sahai E, Zelenay S, Reis e Sousa C (2018) NK cells stimulate recruitment of cDC1 into the tumor microenvironment promoting cancer immune control. *Cell* 172: 1022–1037.e1014
- Castro I, Yu A, Dee MJ, Malek TR (2011) The basis of distinctive IL-2- and IL-15-dependent signaling: weak CD122-dependent signaling favors CD8⁺ T central-memory cell survival but not T effector-memory cell development. *J Immunol* 187: 5170–5182
- Conlon KC, Lugli E, Welles HC, Rosenberg SA, Fojo AT, Morris JC, Fleisher TA, Dubois SP, Perera LP, Stewart DM et al (2015) Redistribution, hyperproliferation, activation of natural killer cells and CD8 T cells, and cytokine production during first-in-human clinical trial of recombinant human interleukin-15 in patients with cancer. *J Clin Oncol* 33: 74–82
- Dolstra H, Roeven MWH, Spanholtz J, Hangalapura BN, Tordoir M, Maas F, Leenders M, Bohme F, Kok N, Trilsbeek C et al (2017) Successful transfer of umbilical cord blood CD34(+) hematopoietic stem and progenitor-derived NK cells in older acute myeloid leukemia patients. *Clin Cancer Res* 23: 4107–4118
- Dybkaer K, Iqbal J, Zhou G, Geng H, Xiao L, Schmitz A, d'Amore F, Chan WC (2007) Genome wide transcriptional analysis of resting and IL2 activated human natural killer cells: gene expression signatures indicative of novel molecular signaling pathways. *BMC Genom* 8: 230
- Fior R, Povoja V, Mendes RV, Carvalho T, Gomes A, Figueiredo N, Ferreira MG (2017) Single-cell functional and chemosensitive profiling of combinatorial colorectal therapy in zebrafish xenografts. *Proc Natl Acad Sci USA* 114: E8234–E8243
- Fujii R, Jochems C, Tritsch SR, Wong HC, Schlom J, Hodge JW (2018) An IL-15 superagonist/IL-15R α fusion complex protects and rescues NK cell-cytotoxic function from TGF- β 1-mediated immunosuppression. *Cancer Immunol Immunother* 67: 675–689
- Gabrilovich DI, Nagaraj S (2009) Myeloid-derived suppressor cells as regulators of the immune system. *Nat Rev Immunol* 9: 162–174
- Gwinn DM, Shackelford DB, Egan DF, Mihaylova MM, Mery A, Vasquez DS, Turk BE, Shaw RJ (2008) AMPK phosphorylation of raptor mediates a metabolic checkpoint. *Mol Cell* 30: 214–226
- Harjunpaa H, Lloret Asens M, Guenther C, Fagerholm SC (2019) Cell adhesion molecules and their roles and regulation in the immune and tumor microenvironment. *Front Immunol* 10: 1078
- Harris SG, Padilla J, Koumas L, Ray D, Phipps RP (2002) Prostaglandins as modulators of immunity. *Trends Immunol* 23: 144–150
- Hason M, Bartunek P (2019) Zebrafish models of cancer—new insights on modeling human cancer in a non-mammalian vertebrate. *Genes (Basel)* 10: 935
- Holt D, Ma X, Kundu N, Fulton A (2011) Prostaglandin E₂ (PGE₂) suppresses natural killer cell function primarily through the PGE₂ receptor EP4. *Cancer Immunol Immunother* 60: 1577–1586
- Hu CD, Kosaka Y, Marcus P, Rashedi I, Keating A (2019) Differential immunomodulatory effects of human bone marrow-derived mesenchymal stromal cells on natural killer cells. *Stem Cells Dev* 28: 933–943
- Huntington ND, Cursons J, Rautela J (2020) The cancer–natural killer cell immunity cycle. *Nat Rev Cancer* 20: 437–454
- Huse M (2017) Mechanical forces in the immune system. *Nat Rev Immunol* 17: 679–690
- Jewell JL, Fu V, Hong AW, Yu FX, Meng D, Melick CH, Wang H, Lam WM, Yuan HX, Taylor SS et al (2019) GPCR signaling inhibits mTORC1 via PKA phosphorylation of Raptor. *Elife* 8: e43038
- Kennedy MK, Glaccum M, Brown SN, Butz EA, Viney JL, Embers M, Matsuki N, Charrier K, Sedger L, Willis CR et al (2000) Reversible defects in natural killer and memory CD8 T cell lineages in interleukin 15-deficient mice. *J Exp Med* 191: 771–780
- Kim DU, Nam J, Cha MD, Kim SW (2019) Inhibition of phosphodiesterase 4D decreases the malignant properties of DLD-1 colorectal cancer cells by repressing the AKT/mTOR/Myc signaling pathway. *Oncol Lett* 17: 3589–3598
- Lee H, Quek C, Silva I, Tasker A, Batten M, Rizos H, Lim SY, Nur Gide T, Shang P, Attrill GH et al (2019) Integrated molecular and immunophenotypic analysis of NK cells in anti-PD-1 treated metastatic melanoma patients. *Oncoimmunology* 8: e1537581
- Li T, Zhang Q, Jiang Y, Yu J, Hu Y, Mou T, Chen G, Li G (2016) Gastric cancer cells inhibit natural killer cell proliferation and induce apoptosis via prostaglandin E₂. *Oncoimmunology* 5: e1069936
- Li H, Fan C, Feng C, Wu Y, Lu H, He P, Yang X, Zhu F, Qi Q, Gao Y et al (2019) Inhibition of phosphodiesterase-4 attenuates murine ulcerative colitis through interference with mucosal immunity. *Br J Pharmacol* 176: 2209–2226

- Liao W, Lin JX, Leonard WJ (2011) IL-2 family cytokines: new insights into the complex roles of IL-2 as a broad regulator of T helper cell differentiation. *Curr Opin Immunol* 23: 598–604
- Liu SJ, Yan DC (2000) ICAM-1 (CD54) expression on T lymphocytes and natural killer cells from umbilical cord blood: regulation with interleukin-12 and interleukin-15. *Cytokines Cell Mol Ther* 6: 161–164
- Liu L, Ge D, Ma L, Mei J, Liu S, Zhang Q, Ren F, Liao H, Pu Q, Wang T et al (2012) Interleukin-17 and prostaglandin E2 are involved in formation of an M2 macrophage-dominant microenvironment in lung cancer. *J Thorac Oncol* 7: 1091–1100
- Liu E, Tong Y, Dotti G, Shaim H, Savoldo B, Mukherjee M, Orange J, Wan X, Lu X, Reynolds A et al (2018) Cord blood NK cells engineered to express IL-15 and a CD19-targeted CAR show long-term persistence and potent antitumor activity. *Leukemia* 32: 520–531
- Manning CD, Burman M, Christensen SB, Cieslinski LB, Essayan DM, Grous M, Torphy TJ, Barnette MS (1999) Suppression of human inflammatory cell function by subtype-selective PDE4 inhibitors correlates with inhibition of PDE4A and PDE4B. *Br J Pharmacol* 128: 1393–1398
- Mao Y, van Hoef V, Zhang X, Wennerberg E, Lorent J, Witt K, Masvidal L, Liang S, Murray S, Larsson O et al (2016) IL-15 activates mTOR and primes stress-activated gene expression leading to prolonged antitumor capacity of NK cells. *Blood* 128: 1475–1489
- Marcais A, Cherfils-Vicini J, Viant C, Degouve S, Viel S, Fenis A, Rabilloud J, Mayol K, Tavares A, Bienvenu J et al (2014) The metabolic checkpoint kinase mTOR is essential for IL-15 signaling during the development and activation of NK cells. *Nat Immunol* 15: 749–757
- Marcais A, Marotel M, Degouve S, Koenig A, Fauteux-Daniel S, Drouillard A, Schlums H, Viel S, Besson L, Allatif O et al (2017) High mTOR activity is a hallmark of reactive natural killer cells and amplifies early signaling through activating receptors. *Elife* 6: e26423
- Neo SY, Yang Y, Record J, Ma R, Chen X, Chen Z, Tobin NP, Blake E, Seitz C, Thomas R et al (2020) CD73 immune checkpoint defines regulatory NK cells within the tumor microenvironment. *J Clin Invest* 130: 1185–1198
- Ni J, Wang X, Stojanovic A, Zhang Q, Wincher M, Buhler L, Arnold A, Correia MP, Winkler M, Koch PS et al (2020) Single-cell RNA sequencing of tumor-infiltrating NK cells reveals that inhibition of transcription factor HIF-1 α unleashes NK cell activity. *Immunity* 52: 1075–1087.e8
- Ogawa F, Amano H, Ito Y, Matsui Y, Hosono K, Kitasato H, Satoh Y, Majima M (2014) Aspirin reduces lung cancer metastasis to regional lymph nodes. *Biomed Pharmacother* 68: 79–86
- Park A, Lee Y, Kim MS, Kang YJ, Park YJ, Jung H, Kim TD, Lee HG, Choi I, Yoon SR (2018) Prostaglandin E2 secreted by thyroid cancer cells contributes to immune escape through the suppression of natural killer (NK) cell cytotoxicity and NK cell differentiation. *Front Immunol* 9: 1859
- Passweg JR, Tichelli A, Meyer-Monard S, Heim D, Stern M, Kuhne T, Favre G, Gratwohl A (2004) Purified donor NK-lymphocyte infusion to consolidate engraftment after haploidentical stem cell transplantation. *Leukemia* 18: 1835–1838
- Peng Y, Li Y, Tian Y, Ao G (2018) PDE4a predicts poor prognosis and promotes metastasis by inducing epithelial-mesenchymal transition in hepatocellular carcinoma. *J Cancer* 9: 2389–2396
- Pradier A, Tabone-Eglinger S, Huber V, Bosshard C, Rigal E, Wehrle-Haller B, Roosnek E (2014) Peripheral blood CD56(bright) NK cells respond to stem cell factor and adhere to its membrane-bound form after upregulation of c-kit. *Eur J Immunol* 44: 511–520
- Pullamsetti SS, Banat GA, Schmall A, Szibor M, Pomagruk D, Hanze J, Kolosionek E, Wilhelm J, Braun T, Grimminger F et al (2013) Phosphodiesterase-4 promotes proliferation and angiogenesis of lung cancer by crosstalk with HIF. *Oncogene* 32: 1121–1134
- Qiao J, Fu Y-X (2020) Cytokines that target immune killer cells against tumors. *Cell Mol Immunol* 17: 722–727
- Reinders ME, Hoogduijn MJ (2014) NK Cells and MSCs: possible implications for MSC therapy in renal transplantation. *J Stem Cell Res Ther* 4: 1000166
- Ring AM, Lin JX, Feng D, Mitra S, Rickert M, Bowman GR, Pande VS, Li P, Moraga I, Spolski R et al (2012) Mechanistic and structural insight into the functional dichotomy between IL-2 and IL-15. *Nat Immunol* 13: 1187–1195
- Roederer M, Nozzi JL, Nason MC (2011) SPICE: exploration and analysis of post-cytometric complex multivariate datasets. *Cytometry A* 79: 167–174
- Roy J, Audette M, Tremblay MJ (2001) Intercellular adhesion molecule-1 (ICAM-1) gene expression in human T cells is regulated by phosphotyrosyl phosphatase activity. Involvement of NF-kappaB, Ets, and palindromic interferon-gamma-responsive element-binding sites. *J Biol Chem* 276: 14553–14561
- Ruggeri L, Mancusi A, Burchielli E, Capanni M, Carotti A, Aloisi T, Aversa F, Martelli MF, Velardi A (2008) NK cell alloreactivity and allogeneic hematopoietic stem cell transplantation. *Blood Cells Mol Dis* 40: 84–90
- Schmetterer KG, Goldhahn K, Ziegler LS, Gerner MC, Schmidt RL, Themanns M, Zebelin-Brandl E, Trapin D, Leitner J, Pickl WF et al (2019) Overexpression of PDE4A acts as checkpoint inhibitor against cAMP-mediated immunosuppression *in vitro*. *Front Immunol* 10: 1790
- Shaffer BC, Le Lueduc JB, Forlenza C, Jakubowski AA, Perales MA, Young JW, Hsu KC (2016) Phase II study of haploidentical natural killer cell infusion for treatment of relapsed or persistent myeloid malignancies following allogeneic hematopoietic cell transplantation. *Biol Blood Marrow Transplant* 22: 705–709
- Solinas G, Schiarea S, Liguori M, Fabbri M, Pesce S, Zammataro L, Pasqualini F, Nebuloni M, Chiabrando C, Mantovani A et al (2010) Tumor-conditioned macrophages secrete migration-stimulating factor: a new marker for M2-polarization, influencing tumor cell motility. *J Immunol* 185: 642–652
- Souza-Fonseca-Guimaraes F, Cursons J, Huntington ND (2019) The emergence of natural killer cells as a major target in cancer immunotherapy. *Trends Immunol* 40: 142–158
- Sun R, Fan J, Wei H, Zhang C, Tian Z (2003) Use of interleukin-15 for preparation of adherent NK cells from human peripheral blood: comparison with interleukin-2. *J Immunol Methods* 279: 79–90
- Tang Z, Kang B, Li C, Chen T, Zhang Z (2019) GEPIA2: an enhanced web server for large-scale expression profiling and interactive analysis. *Nucleic Acids Res* 47: W556–W560
- Wang F, Meng M, Mo B, Yang Y, Ji Y, Huang P, Lai W, Pan X, You T, Luo H et al (2018) Crosstalks between mTORC1 and mTORC2 variate cytokine signaling to control NK maturation and effector function. *Nat Commun* 9: 4874
- Wennerberg E, Pfefferle A, Ekblad L, Yoshimoto Y, Kremer V, Kaminsky VO, Juhlin CC, Hoog A, Bodin I, Svjataho V et al (2014) Human anaplastic thyroid carcinoma cells are sensitive to NK cell-mediated lysis via ULBP2/5/6 and chemoattract NK cells. *Clin Cancer Res* 20: 5733–5744
- Woo EY, Chu CS, Goletz TJ, Schlienger K, Yeh H, Coukos G, Rubin SC, Kaiser LR, June CH (2001) Regulatory CD4(+)CD25(+) T cells in tumors from patients with early-stage non-small cell lung cancer and late-stage ovarian cancer. *Cancer Res* 61: 4766–4772
- Yan C, Brunson DC, Tang Q, Do D, Ifimia NA, Moore JC, Hayes MN, Welker AM, Garcia EG, Dubash TD et al (2019) Visualizing engrafted human

- cancer and therapy responses in immunodeficient zebrafish. *Cell* 177: 1903–1914.e1914
- Zelenay S, van der Veen AG, Bottcher JP, Snelgrove KJ, Rogers N, Acton SE, Chakravarty P, Girotti MR, Marais R, Quezada SA et al (2015) Cyclooxygenase-dependent tumor growth through evasion of immunity. *Cell* 162: 1257–1270
- Zhang X, Sun S, Hwang I, Tough DF, Sprent J (1998) Potent and selective stimulation of memory-phenotype CD8⁺ T cells *in vivo* by IL-15. *Immunity* 8: 591–599
- Zhang J, Sun R, Wei H, Zhang J, Tian Z (2004) Characterization of interleukin-15 gene-modified human natural killer cells: implications for adoptive cellular immunotherapy. *Haematologica* 89: 338–347
- Zheng R, Wan C, Mei S, Qin Q, Wu Q, Sun H, Chen CH, Brown M, Zhang X, Meyer CA et al (2019a) Cistrome data browser: expanded datasets and new tools for gene regulatory analysis. *Nucleic Acids Res* 47: D729–D735
- Zheng X, Qian Y, Fu B, Jiao D, Jiang Y, Chen P, Shen Y, Zhang H, Sun R, Tian Z et al (2019b) Mitochondrial fragmentation limits NK cell-based tumor immunosurveillance. *Nat Immunol* 20: 1656–1667
- Zhong J, Xie J, Xiao J, Li D, Xu B, Wang X, Wen H, Zhou Z, Cheng Y, Xu J et al (2019) Inhibition of PDE4 by FCPR16 induces AMPK-dependent autophagy and confers neuroprotection in SH-SY5Y cells and neurons exposed to MPP(+)-induced oxidative insult. *Free Radic Biol Med* 135: 87–101



License: This is an open access article under the terms of the Creative Commons Attribution-NonCommercial License, which permits use, distribution and reproduction in any medium, provided the original work is properly cited and is not used for commercial purposes.